Nat Hazards (2013) 68:1075–1087
DOI 10.1007/s11069-013-0675-1

ORIGINAL PAPER

Paleoseismic study of the east Kalpintage fault in southwest Tianshan based on deformation of alluvial fans and ^{10}Be dating

An Li · Yongkang Ran · Liangxin Xu · Huaguo Liu

Received: 6 January 2013 / Accepted: 1 April 2013 / Published online: 18 April 2013

Abstract Multiple earthquakes produced by thrusting deformation have been recorded over the last century in the Tianshan area. Paleoseismic studies are very important in the exploration of the active quaternary tectonics and the risk assessment of great earthquakes in the Tianshan orogenic region. However, in this area, paleoseismic research is still lacking because of the lack of samples dated by ^{14}C or optically stimulated luminescence (OSL) methods. We determined the ages of the alluvial fans by ^{10}Be terrestrial cosmogenic nuclide (TCN) dating, measured the surface deformation of the fault scarp in a GPS survey, and evaluated the vertical displacements of the events in trenches in the east Kalpintage fault in the southwest Tianshan region. We estimated the displacement and recurrence intervals of the paleoseismic events and constrained the errors of the ^{10}Be ages and slip rates using a Monte Carlo simulation method. Our study suggests that each paleoseismic event shows a similar displacement of $\sim$1.5 m with a recurrence interval of $\sim$5 kyr in the east Kalpintage fault. The calculated slip rate is 0.31(+0.21/−0.18) mm/yr. In such arid regions with large areas of coarse gravel that lack ^{14}C or OSL samples, the integration of TCN dating, geomorphic deformation survey, and trenching methods is a reliable alternative for studying the active regional tectonics.

Keywords Paleoseismic event · Fault scarp · ^{10}Be exposure age · Monte Carlo simulation

This study was supported by the National Natural Science Foundation of China (40872130).

A. Li · Y. Ran (✉) · L. Xu
Key Laboratory of Active Tectonics and Volcano, Institute of Geology,
China Earthquake Administration, Beijing 100029, China
e-mail: ykran@263.net

A. Li
e-mail: antares_lee@163.com

L. Xu
e-mail: s0mile0@163.com

H. Liu
China Earthquake Disaster Prevention Center, Beijing 100029, China
e-mail: cedpclhg@163.com

1 Introduction

Tianshan, one of the largest orogenic belts in the Eurasian continent, has experienced several M8 and multiple M7 earthquakes since the beginning of the twentieth century (the earthquake catalog of China 2000). The multiple earthquakes in the Tianshan region were produced by thrust faults. Paleoseismic studies provide important information on the active quaternary tectonics and the risk of great earthquakes in the Tianshan orogenic region. However, paleoseismic studies on thrust faults are not as well conducted as those on normal or strike-slip faults in the Chinese mainland. Because the main material deposited in alluvial fans at the foot of the fault-fold belt is gravel and there is a lack of ^{14}C datable samples and optically stimulated luminescence (OSL) samples, there are uncertainties in the paleoseismic studies in the region. However, multi-level alluvial fans have developed in the intensely uplifted area, and the thrust fault shows different heights of fault scarps on these fans. The higher scarps indicate that earthquakes occurred after the older alluvial fan developed. We attempt to put constraints on the timing of the various paleoseismic events and estimate the average slip rate and recurrence interval of the earthquakes by determining the fault displacements and the ages of the alluvial fans. Terrestrial cosmogenic nuclide (TCN) dating is a key technique for determining paleoseismic time in this arid area. The advantages of ^{10}Be nuclide dating are its suitability for sampling and the high reliability of the estimated exposure age of the alluvial fans in the arid area (Lal 1991; Gosse and Phillips 2001). Bierman (1995) tried to estimate the timing of boulder deposition and abandonment of the faulted fan by TCN dating and calculated the average recurrence interval of the surface ruptures on the alluvial fan in Owens valley. Their result was based on two assumptions: that the influence of the inherited nuclide concentration was negligible and that the displacements created on the surface of the alluvial fans by the various earthquakes were similar. Because ^{10}Be depth profile dating has improved in recent years, the exposure age of the alluvial fans can be determined more accurately and the errors of the age can be more reliably estimated by Monte Carlo simulation method. We conducted a paleoseismic study in the Tianshan area using the latest ^{10}Be TCN dating technology.

The Kalpin thrust system is a well-known multi-row thrust system in southwest Tianshan, near the northeast margin of the Pamir Plateau range. Earthquakes occur frequently in this area. For example, there were nine M6–7 earthquakes during 1997–1998 and the Bachu-Jiashi Ms 6.8 earthquake was recorded in 2003. The Atushi M8.5 earthquake occurred on the west side of the Kalpin in 1902. Thus, the Kalpin system experienced a high number of strong earthquakes in recent years including a very large one. Quaternary tectonic activity is very evident along the Kalpin thrust system. The multi-level alluvial fans and fault scarps are important objects for paleoseismic study of the active tectonics in the Kalpin system. The research site was chosen for its multi-level alluvial fans and multi-level fault scarps. We determined the age of the alluvial fans by ^{10}Be TCN dating, the deformation of the fault scarps by GPS surveying, and the displacement of the paleoseismic events by a geomorphic trench survey. With the combination of the data obtained, we estimated the interval and slip rate of the great earthquakes that left their mark on our study site.

2 Paleoearthquakes

2.1 Study area

The Kalpin thrust system locates on the northwest margin of the Tarim Basin. In this region, emergent thrust sheets are predominantly verge toward the interior of the Tarim

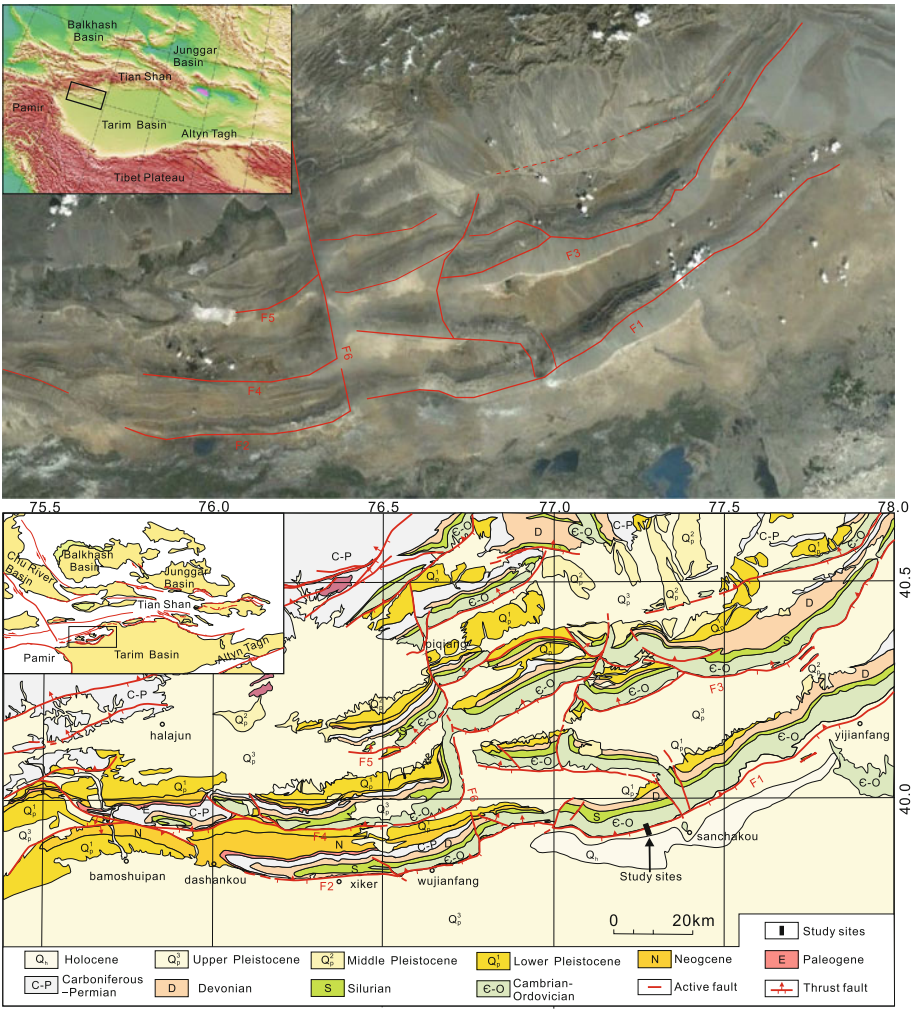

Fig. 1 Satellite image and regional tectonics of the Kalpin thrust system. *F1* east Kalpintage fault, *F2* west Kalpintage fault, *F3* Saergantage fault, *F4* aozigertawutage fault, *F5* tuokesanatanengbaile fault, *F6* piqiang fault

Basin to the south (Yeats et al. 1997; Allen et al. 1999; Xu et al. 2006). Strata crop out in elongate ridges in the hanging wall of each thrust. Spacing between these ridges is typically 10–20 km (Fig. 1). There is a major stratigraphic gap between the lower Permian and lower Miocene to Quaternary clastic rocks (Allen et al. 1999). The seismic reflection profile shows the detachment layer is 4 km deep and faults are dip to NNW with 12–15° in the east Kalpin thrust system (Yang et al. 2010). The smooth variation of bedding dip in the emergent sections suggests fault propagation folding rather than the planar ramps and flats which would be produced as a result of fault bend folding. A balanced section across zone indicates ∼28 % shortening, equivalent to ∼35 km. This is equivalent to an average slip rate of ∼1.8 mm/year, assuming deformation began at circa 20 Ma in whole Kalpin system (Allen et al. 1999).

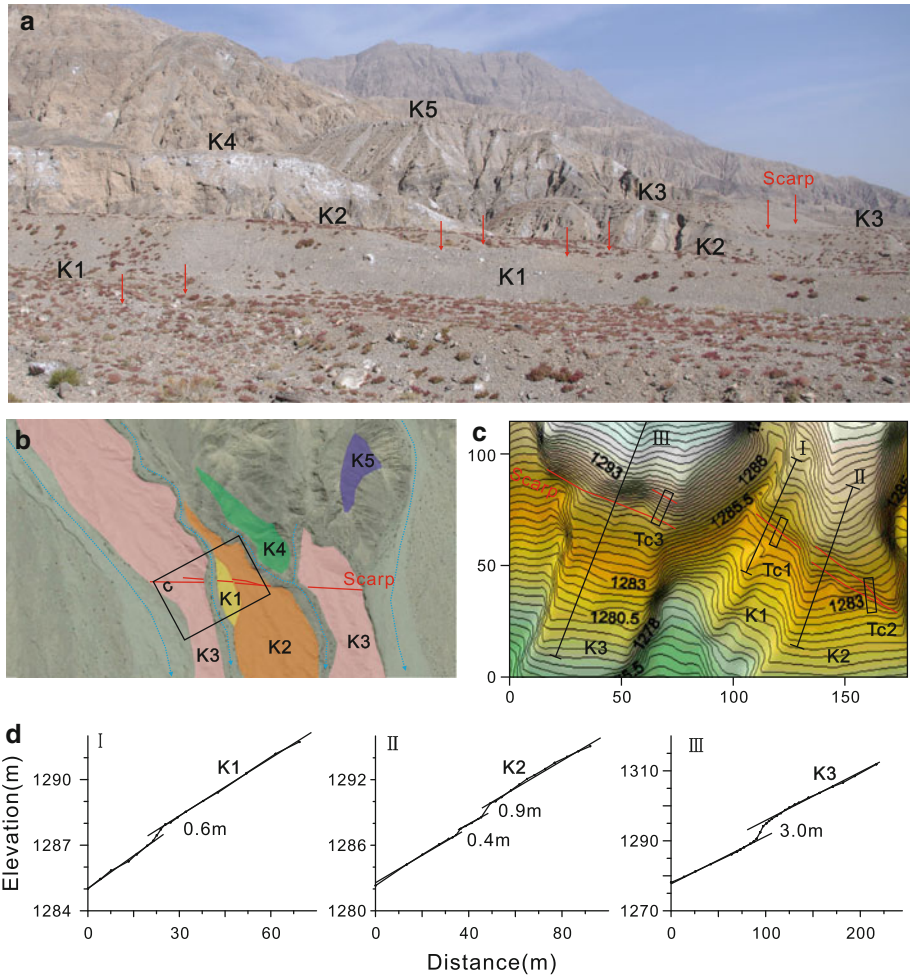

Fig. 2 Geomorphic features of the research site. **a** Photograph of the study site looking northeast; *K1–K5* are the alluvial fans, *red arrows* show the fault site; **b** image interpretation, *black frame* is the range shown in **c**; **c** the measured topographic map, *black frames* are sites of trenches *Tc1–Tc3*, *black lines* are profiles I–III in **d**; **d** topographic profiles of the *K1–K3* alluvial fans

The Piqiang fault divides the Kalpin system into two segments: eastern and western. Each segment has developed a multi-row thrust fault-fold belt. Our research site, northwest of Sanchakou, is located in the middle of east Kalpintage (the southeast mountain of the Kalpin system). The site (N39°56′46″; E78°16′51″) is located at the highest point of the arcuate structure in the eastern section (Fig. 1). Five-level alluvial fans exist in the research site (from lowest to highest: K1, K2, K3, K4, and K5). The main sediment of all the alluvial fans is gravel. Fault scarps appear at different heights on the three lower alluvial fans. The geomorphic surfaces of the footwall and the hanging wall are well preserved on K1, K2, and K3. In the K4 and K5 alluvial fans, only the surface of the hanging wall has been preserved. The elevations of the alluvial fans above the gully are 1.5, 3.7, 8.9, 20.8, and 37.2 m from K1 to K5. The heights of the fault scarps are 0.6, 1.3, and 3.0 m on K1, K2, and K3, respectively. This indicates that more than one paleoseismic event occurred

since these alluvial fans were formed. The hanging wall uplifted when the paleoseismic events occurred; hence, the number of geomorphic surfaces of the hanging wall is more than that of the footwall. We excavated trenches Tc1, Tc2, and Tc3 on the K1, K2, and K3 alluvial fans, respectively (Fig. 2).

2.2 Paleoseismic events

The TC1 trench across the fault scarp on the K1 alluvial fan reveals five units (Fig. 3). U1 is the bedrock. Units U12–U14 are alluvial deposits. U15 is a colluvial wedge. The F4 fault faces north with a dip angle of 20° and ruptures the surface. The vertical deformation of U12–U14 is 0.5–0.6 m, which corresponds to the height of the fault scarp (about 0.6 m) on the K1 alluvial fan. This indicates that only one paleoseismic event occurred since K1 formed. This paleoseismic event is named Event Z. A fault displacement of 1.0–1.2 m is estimated from deformation on the lower boundary of U13 and U14 in Event Z.

The Tc2 trench was excavated across the fault scarp on the K2 alluvial fan. Five units are revealed in the Tc2 trench from the bottom to the top (Fig. 4). U1 is the bedrock. U8–U10 are a series of alluvial deposits and have obviously horizontal bedding. The material of U11 is close to U10, but it is chaotic and unstratified (Fig. 4b). It is a colluvial wedge produced by an earthquake. Two fault planes have been identified in the Tc2 trench. The F3 fault dips north with an angle of 20° and is divided into two planes from the middle of U8 to U10. The strata form S- or Z-shaped folds near the F3 fault. The top of the F3 fault is covered by unit U11 (Fig. 3a). The F4 fault also dips north with an angle of 20°, and the strata near F4 are folded. The F4 fault cuts through the U11 layer to the surface and dislocates U11 (Fig. 3b). On the K2 alluvial fan, the two fault planes correspond to the two scarps, indicating that two paleoseismic events occurred since K2 formed. The F3 fault dislocated units U8–U10 in the first paleoseismic event (defined as Event Y). The F3 displacement of 2.1–2.2 m is calculated from the lower boundaries of U9 and U10 in Event Y. Unit U11 accumulated after Event Y. F4 dislocated unit U11 and ruptured the surface at K2 in the most recent event. Because this event ruptured the surface as Event Z did in the

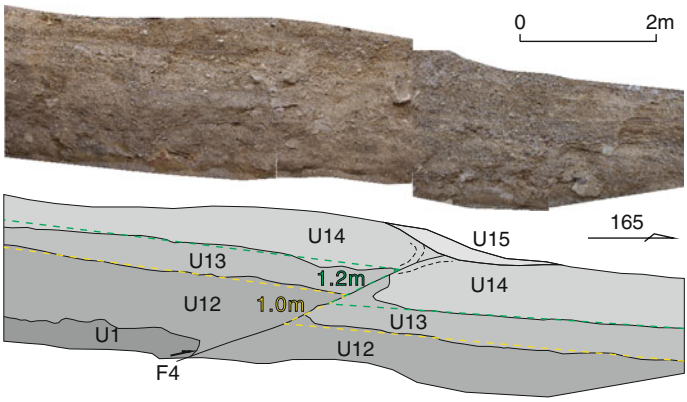

Fig. 3 Tc1 trench. *U1* brown sandy mudstone, *U2* small pebble layer, pebble diameter of 2–3 cm, low psephicity, horizontal bedding, coarse sandy lens. *U3* pebble layer with grain size about 5 cm, low psephicity, horizontal bedding, slight sorting, *U4*: small gravel layer with high sand content, grain size about 2–3 cm smaller than *U3*. The top of *U4* has a high content of clay where salinization occurs easily, *U5* the colluvial wedge of Event A

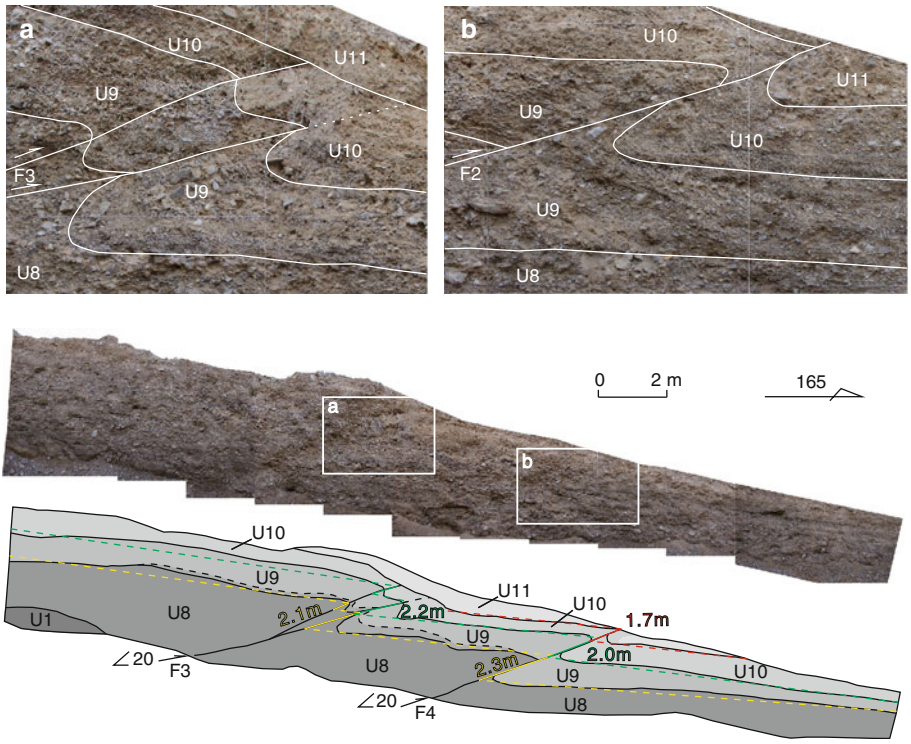

Fig. 4 Tc2 trench. **a** Detailed photograph of the *F1* fault; **b** detailed photograph of the *F2* fault. *U1* brown sandy mudstone. *U2* pebble layer, pebble diameter of 2–10 cm, poor sorting and slight bedding. *U3* pebble layer with grain size about 5–6 cm, high sand content (higher than in *U2*). The small pebble layer with grain size about 1–2 cm in the bottom of *U3* is an important marker layer. It indicates the displacement of the F1 fault. *U4* pebble layer with grain size about 3–5 cm. This layer has a high clay content with salinization and has small pebble lenses with grain size about 1–2 cm. *U5* the long colluvial wedge of a paleoseismic event. Mainly sand with many small pebbles with grain size about 2–3 cm. It is dislocated by the *F2* fault

Tc1 trench, they are considered the same paleoseismic event. The F4 displacement of 1.7–2.3 m was calculated from the lower boundaries of U9, U10, and U11 in the most recent event (Event Z).

The Tc3 trench was excavated at the fault scarp on the K3 alluvial fan. Seven strata units, U2–U7 and U11 from the bottom to the top, are revealed in the Tc3 trench (Fig. 5). Units U2–U5 form a series of alluvial deposit strata. The U3 is a marker bed that records the total displacement of 8.3 m in the Tc3. U2–U5 have obvious horizontal bedding but U6–U7 are unstratified (Fig. 5a). The U6, U7 and U11 colluvial wedges are related to paleoseismic events. Three fault planes are exposed in the Tc3 trench. The F1 fault dips north with an angle of 18–20° and dislocates all the strata and the surface. The F1 fault displaced U4 and U5 by 1.7–2.2 m and U6 by 0.9 m. The colluvial wedge U6 is dislocated. This implies that F1 ruptured twice: shifting 0.8–1.3 m in the first rupture, then rupturing again after U6 was deposited, dislocating 0.9 m. F2 also ruptured twice, dislocating U4 and U5 by 1.8–1.9 m in the first time, then U7 and U11 were deposited and subsequently dislocated by 0.6 m in the second rupture. Unit U11 covers the F3 fault. This fault ruptured only once and displaced U3 and U4 by same displacement of 2.6–2.7 m.

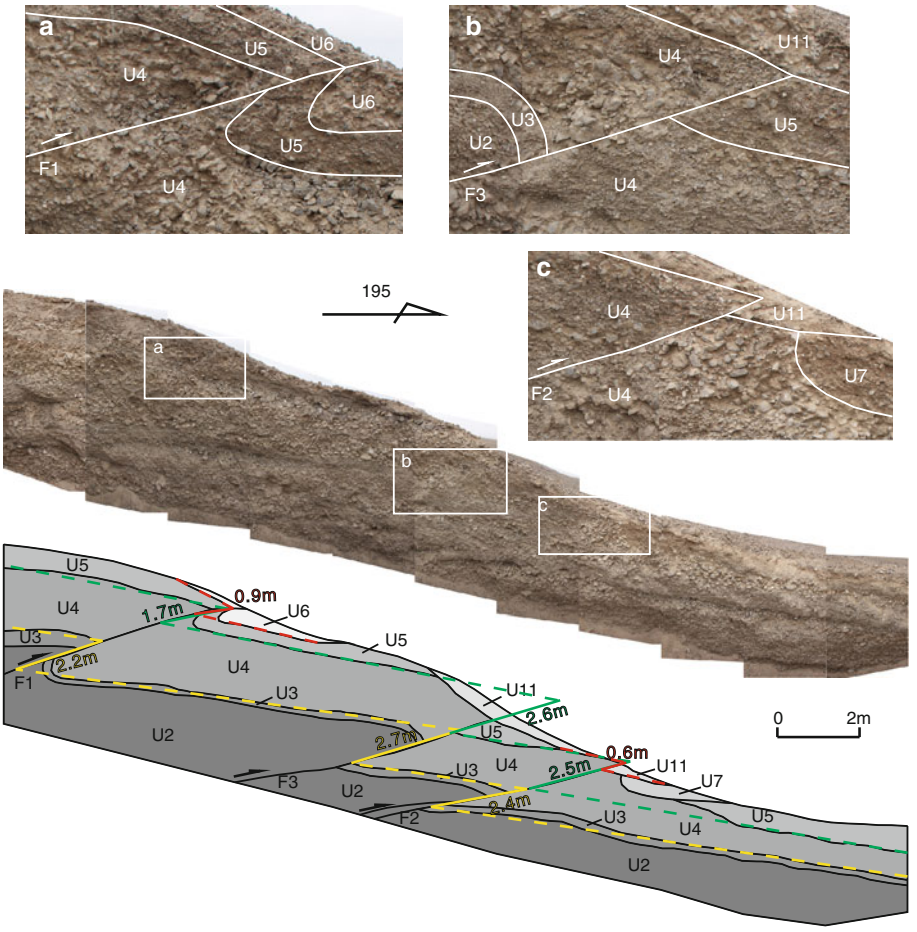

Fig. 5 Tc3 trench. **a** Detailed photograph of the F1 fault; **b** detailed photograph of the F2 fault; **c** detailed photograph of the F3 fault. *U1*: *gray white* coarse pebble layer with grain size about 5–10 cm. *U2* small pebble layer with grain size about 1–2 cm and high sand content, an important marker layer. *U3* coarse layer with grain size about 10 cm, a small pebble layer with grain size about 2–3 cm in the middle of *U3*; *U4* coarse sand layer with small pebbles; *U5* pebble colluvial wedge; U6: coarse sand colluvial wedge with some pebbles; *U7 yellow pebble* colluvial with high clay content

Combining the information on the displacements found at trenches Tc1 and Tc2, we recognized four events that occurred in trench Tc3.

Event Z: this is the most recent paleoseismic event. It occurred after the K1 alluvial fan developed. All the trenches preserved the displacements of Event Z, and it ruptured the surfaces of all the alluvial fans. The fault displacement is 1.0–1.2 m in Tc1 and 1.7–2.3 m in Tc2. Both the F1 and F3 faults ruptured the surface with a total displacement of 1.5 m in the Tc3 trench.

Event Y: Tc2 and Tc3 preserved the displacements of this event. The displacement is 2.1–2.2 m in the Tc2 trench and 2.6–2.7 m (F3 displacement) in the Tc3 trench. Because there is no evidence of this event in trench Tc1 on the K1 alluvial fan, we firmly believe that Event Y occurred before the K1 alluvial fan developed. The timing of Event Y is

confined between the ages of K1 and K2. We did not find another paleoseismic event older than Event Y in the Tc2 trench indicating that Event Y was the only event that occurred in the period between the formation of K1 and K2.

Events W and X: fault F1 dislocated U2–U5 in Event X and fault F2 dislocated U2–U5 in Event W. The two events occurred in the period between the formation of K2 and K3 but the time sequence of the events is not confirmed in trench Tc3 by the cut–cover relationship between the faults and the strata. Three factors suggest that Event W and Event X are independent events. (1) The material of the colluvial wedges: the U6 and U7 colluvial wedges were formed after Events W and X, respectively. The deposits of the two colluvial wedges are obviously different. U6 consists mainly of pebbles while U7 contains mostly sand. On the other hand, pebbles are not easy to stop on the fault scrap in earthquake. Always, pebbles roll down the fault scrap. So there is no scrap in front of the U6 when the event W happened. The fault scrap extends to forward in earthquake events X, Y, and Z. (2) The displacements of the events: the displacements of Events Z and Y are about 1.5–2.0 m. If Events W and X were the same earthquake, the total displacement would be almost 3 m—twice as much as that of Events Z and Y. (3) If only one earthquake occurred between 6.8 and 21.5 kyr (see age estimates below), the interval would be much longer than the interval of Events Z and Y (dated between 1.7 and 6.8 kyr). Therefore, we tend to identify Event W and Event Z as two different paleoseismic events with respective displacements of 1.8–1.9 m and 0.8–1.3 m.

2.3 Event dating

The gravel of the alluvial fans in the research site consists mainly of dolomite limestone with small amounts of chalcedony. Hence, we collected surface samples with 40–50 chalcedony pebbles. The grain size of each pebble was less than 2.5 cm, and the top of each pebble has dark-brown rock varnish. All the samples were collected on the hanging wall where the relief is smooth and wide. The sample site is located on the southern side of the Kalpintage range. The mountain does not provide much shade over the area. It is easy to correct the ^{10}Be production rate. The average temperature of the Kalpin area in winter is above freezing point, and the average rainfall is only $\sim$50 mm per year. Therefore, the effects of erosion, snow-cover, and frost heaving can be ignored.

Depth profile samples were collected at depths of 25–225 cm in the Tc1–Tc3 trenches (Fig. 6). The sediment of the alluvial fans has several characteristics: clear horizontal bedding, rapid accumulation, non-depositional hiatus, and a non-mixing effect. This makes it very suitable for depth profile sampling. We collected four unequal interval samples between the depths of 25 and 225 cm for all the depth profiles. The material sampled was coarse sand with a grain size of 0.2–0.6 mm. Each sample weighed 2.5–3 kg and was 300 cm long (horizontally) and 10 cm thick (vertically) (Fig. 6).

Depth profiling of ^{10}Be TCN dating is based on the function that defines the relationship between the concentration and production rate of the ^{10}Be nuclide (Gosse and Phillips 2001). The concentration is detected by accelerator mass spectrometry (AMS) and can estimate accurately the nuclide production rate under different irradiation conditions: altitude, latitude, shielding, magnetic field, and air-pressure (Lal 1991; Dunai 2000; Stone 2000). The C concentration (atoms g^{-1}) for a specific nuclide m as a function of depth z (cm), exposure time t (a), and erosion rat ε (cm a^{-1}) can be written as follows (Hidy et al. 2010). The Monte Carlo simulator can help devise sampling strategies for TCN depth profiles in the MatlabTM graphical user interface (Hidy et al. 2010). The analysis of the distribution with depth of the nuclide concentrations in the depth profile samples is useful

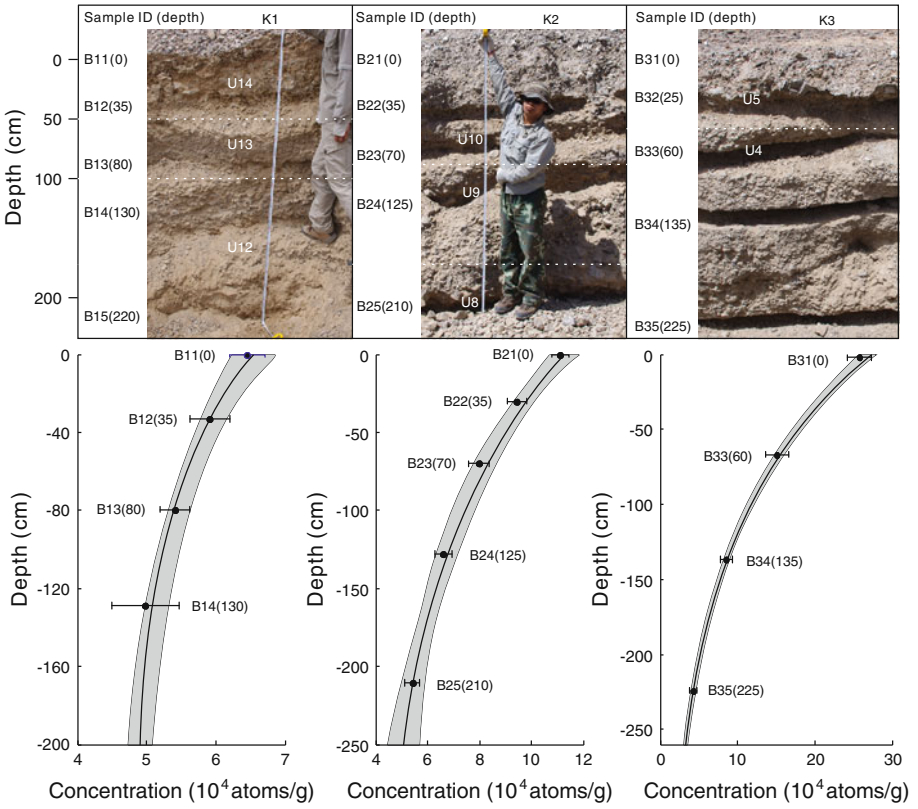

Fig. 6 Photographs of sampling for TCN dating and results of the Monte Carlo simulations for the ^{10}Be nuclide concentrations. The *gray band* is the fitted curve range; the *black curve* is the best result of the fitted value

for determining both the exposure ages and inherited concentrations in a variety of geomorphic settings (Anderson et al. 1996).

$$C_m(z,\varepsilon,t) = \sum_i \frac{P(0)_{m,i}}{\left(\frac{\varepsilon\rho_z}{\Lambda_i}+\lambda_m\right)} \times \exp\left(-\frac{z\rho_z}{\Lambda_i}\right) \times \left[1-\exp\left(-t\left(\frac{\varepsilon\rho_z}{\Lambda_i}+\lambda_m\right)\right)\right] + C_{\mathrm{inh},m} \times \exp(-\lambda_m t)$$

In this relationship, i represents the various sources for nuclide m (neutron spallation, fast muon spallation, and negative muon capture), $P(0)_{m,i}$ is the site-specific surface production rate for nuclide m via production pathway i (atoms g^{-1} a^{-1}), λ_m is the decay constant for radionuclide m (a^{-1}), ρ_z is the cumulative bulk density at depth z (g cm^{-3}), Λ_i is the attenuation length of production pathway i (g cm^{-2}), and $C_{\mathrm{inh},m}$ is the inherited (depositional) concentration of nuclide m (atoms g^{-1} a^{-1}).

All the samples were process at SKLED (State Key Laboratory of Earthquake Dynamics, China), and the AMS measurements were completed at LNNC (Laboratatoire National des Nucleides Cosmogeniques, France). The results of the ^{10}Be concentrations are presented in the Table 1.

Table 1 Results of ^{10}Be depth profiling

Data sample	Site	Grain size (mm)	Depth (cm)	Lat (°)	Lon (°)	Height (m)	P_0 (atoms/g year)	Concentration (10^4 atoms/g)	Quartz weight (g)	Age (kyr)
B11	K1	25	0	39.933	78.267	1,287	11.52	6.5 ± 0.2	27.984	1.7 (+1.0/−0.7)
B12	K1	0.25–0.60	35	39.933	78.267	1,287	8.88	5.8 ± 0.3	35.684	
B13	K1	0.25–0.60	80	39.933	78.267	1,287	6.45	5.4 ± 0.2	37.456	
B14	K1	0.25–0.60	130	39.933	78.267	1,287	4.76	4.9 ± 0.5	14.135	
B15	K1	0.25–0.60	220	39.933	78.267	1,287	3.09	15.1 ± 0.6	19.545	
B21	K2	25	0	39.933	78.267	1,295	11.59	11.1 ± 0.3	40.016	6.8 (+1.5/−2.4)
B22	K2	0.25–0.60	35	39.933	78.267	1,295	8.98	9.5 ± 0.4	21.704	
B23	K2	0.25–0.60	70	39.933	78.267	1,295	7.00	8.0 ± 0.3	37.721	
B24	K2	0.25–0.60	125	39.933	78.267	1,295	4.99	6.6 ± 0.3	24.696	
B25	K2	0.25–0.60	210	39.933	78.267	1,295	3.30	5.4 ± 0.3	37.819	
B31	K3	25	0	39.933	78.267	1,303	11.66	25.7 ± 0.9	40.145	21.5 (+1.5/−2.7)
B32	K3	0.25–0.60	25	39.933	78.267	1,303	–	Cancel	–	
B33	K3	0.25–0.60	60	39.933	78.267	1,303	7.54	15.2 ± 0.7	18.237	
B34	K3	0.25–0.60	135	39.933	78.267	1,303	4.75	7.5 ± 0.3	26.705	
B35	K3	0.25–0.60	225	39.933	78.267	1,303	3.12	4.5 ± 0.2	35.004	

All samples as well as a process blank were normalized with AMS standard KNSTD3110, and the ^{10}Be/^{9}Be ratios were calculated using a ^{10}Be half-life of 1.387 myr. ^{10}Be contribution from blank: 2.67×10^5 atoms (sand samples), 5.4×10^5 atoms (pebble samples)

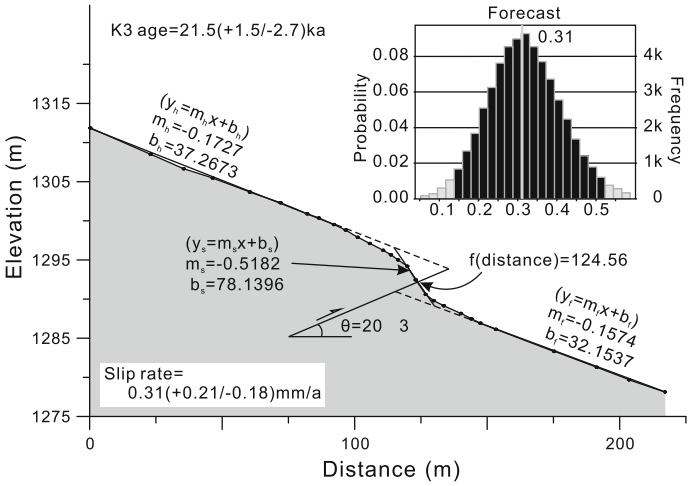

Fig. 7 Calculation of the fault slip rate. $y_h = m_h x + b_h$: the hanging wall tread; $y_s = m_s x + b_s$: scarp face; $y_f = m_f x + b_f$: footwall tread; θ fault dip, f fault position (distance). *Bar graph* the result of the Monte Carlo simulation

Because the quartz weight of sample B32 was too small, the test of this sample was discarded. Fourteen ^{10}Be concentrations were measured. Because of an abnormal high value, the concentration of B15 was eliminated in the calculation of the K1 depth profile. We obtained the depth profiles of K1–K3 by 10 k times of the sampling strategies with the Monte Carlo simulator (Fig. 6) and the exposure ages of the K1–K3 alluvial fans (Table 1).

The calculation procedure was downloaded from: http://geochronology.earthsciences.dal.ca/downloads-models.html.

The exposure age of the three K1–K3 alluvial fans is 1.7 (+1.0/−0.7) kyr, 6.8 (+1.5/−2.4) kyr, and 21.5 (+1.5/−2.7) kyr, respectively. The dates of the four events can be determined from the time sequence of the paleoseismic events and alluvial fans. Event A: present–1.7 (+1.0/−0.7) kyr; Event B: 1.7 (+1.0/−0.7)–6.8 (+1.5/−2.4) kyr. Event C and Event D: 6.8 (+1.5/−2.4)–21.5 (+1.5/−2.7) kyr.

2.4 Fault slip rate

Because the fault deformation is thrusting than folding in trenches (Figs. 3, 4, 5), we used the approach developed by Thompson et al. (2002) for calculating the fault slip from regression parameters fitted to the survey points along the hanging wall tread, scrap face, and footwall tread (Amos et al. 2010). We then used the Monte Carlo approach for estimating the uncertainty associated with the calculated values of fault displacement and slip rate. The Monte Carlo simulation has seen increased use in neotectonic applications where the calculated parameter of interest (fault displacement or slip rate in our case) depends on a large number of variables characterized by either continuous or discrete probability distribution functions (Thompson et al. 2002; Davis et al. 2005; Amos et al. 2010) (Fig. 7). In each calculation, the Monte Carlo simulation associated with each input variable used over 50 K trials to generate a histogram of the calculated parameter of slip rate. The reported values for each output parameter reflect the mode and the 95 % CI of the resulting frequency distributions. The calculated fault slip rate is based on the parameters of the K3 alluvial fan and is 0.31 (+0.21/−0.18) mm/year (Fig. 7).

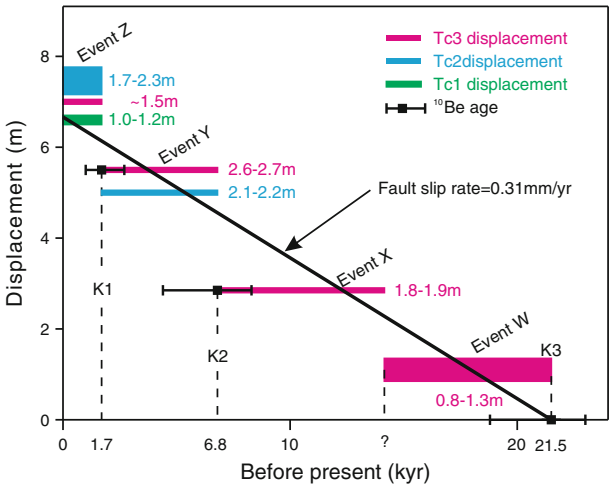

Fig. 8 Paleoseismic events versus the fault slip rate. *Black oblique line* fault slip rate, *red line* displacements in *Tc3*, *blue line* displacements in *Tc2*, *green line* displacement in the *Tc1*

3 Discussion

3.1 Events and slip rate

The calculated fault slip rate of 0.31 mm/year coincides with all the displacements of the paleoseismic events measured in the three trenches (Fig. 8). This demonstrates that the time and displacement of paleoseismic events can be constrained by trench sampling and the exposure age of the alluvial fans. We recognized that multiple earthquakes produced the high fault scarp in the high alluvial fan. There is a positive correlation between the height of the fault scarp and the number of paleoseismic events. The fault displacement calculated with the scarp model of Thompson et al. (2002) is in good agreement with the actual value (measured in the trench). The slip rate of 0.31 mm/year shows a good fit to the displacements of all the events in the three trenches. This slip rate reflects the active intensity of the Kalpintage fault in the Kalpin thrust system.

3.2 The reliability of the events

The majority of the displacements due to paleoseismic events in the east Kalpintage fault showed dislocations of $\sim$1.5 m and occurred over the last 21.5 kyr. The interval between events was $\sim$5 kyr and was calculated by the slip rate. The four paleoseismic events identified from our geomorphic survey and sampling of the three trenches fit this law. The range of the best-fit curve for the nuclide concentration results is very narrow (Fig. 6). This indicates that the alluvial fan ages are highly reliable according to the theoretical model of the depth profile dating. The errors in the estimates of the alluvial fan ages are $\sim$2 kyr by the Monte Carlo simulation (Table 1), which is very small compared with the K3 age of 21.5 kyr. Therefore, the bar graph of the results (Fig. 7) shows that the slip rate which was calculated by the Monte Carlo simulation has a strong convergence between 0.2 and 0.4 mm/year near the median value of 0.31 mm/yr. The result of the slip rate is within the 95 % CIs of the resulting frequency distributions. Compared with the interval for the four

paleoseismic events, the errors in the age estimates are small. Therefore, the displacements of the events fit well with the oblique line of the slip rate (Fig. 8). The events identified in the east Kalpintage fault had similar displacements and intervals. Moreover, in arid areas such as our study site, where the coarse gravel deposits lack ^{14}C samples, a paleoseismic study combined with TCN dating, geomorphic deformation survey, and trench excavation is a favorable alternative for obtaining highly reliable geological date estimates.

4 Conclusions

Based on the paleoseismic analysis and geomorphic deformation mapping in the research site of the east Kalpintage fault, we conclude the following:

(1) The paleoseismic events have similar displacements of $\sim$1.5 m at intervals of $\sim$5 kyr in the east Kalpintage fault. The fault slip rate is 0.31 (+0.21/−0.18) mm/year.
(2) In the arid area that contains large deposits of coarse gravel that lack ^{14}C samples, a paleoseismic study that combines TCN dating with a geomorphic deformation survey and trench excavation is an alternative credible method for dating tectonic activities.

References

Allen MB, Vincent SJ, Wheeler PJ (1999) Late Cenozoic tectonics of the Kepingtage thrust zone: interactions of the Tien Shan and Tarim Basin, northwest China. Tectonics 18(4):639–654

Amos CB, Burbank DW, Read SA (2010) Along-strike growth of the Ostler fault, New Zealand: consequences for drainage deflection above active thrusts. Tectonics, 29: TC4021

Anderson RS, Repka JL, Dick GS (1996) Explicit treatment of inheritance in dating depositional surfaces using in situ 10Be and 26Al. Geology 96:47–51

Bierman PR (1995) Cosmogenic ages for earthquake recurrence intervals and debris flow fan deposition, Owens Valley, California. Science 270:447–450

China earthquake directory edited group (2000) China earthquake directory from BC 780 to AD 1986. Earthquake Press (in Chinese), Beijing

Davis K, Burbank DW, Fisher D et al (2005) Thrust-fault growth and segment linkage in the active Ostler fault zone, New Zealand. J Struct Geol 27(8):1528–1546

Dunai TJ (2000) Scaling factors for production rates of in situ produced cosmogenic nuclides: a critical reevaluation. Earth Planet Sci Lett 176:157–169

Gosse JC, Phillips FM (2001) Terrestrial in situ cosmogenic nuclides theory and application. Quat Sci Rev 20:1475–1560

Hidy AJ, Gosse JC, Pederson JL et al (2010) A geologically constrained Monte Carlo approach to modeling exposure ages from profiles of cosmogenic nuclides: an example from Lees Ferry, Arizona. Geochem Geophys Geosyst 11:Q0AA10.1–18

Lal D (1991) Cosmic ray labeling of erosion surfaces_in situ nuclide production rates and erosion models. Earth Planet Sci Lett 104:424–439

Stone JO (2000) Air pressure and cosmogenic isotope production. J Geophys Res 105:23753–23759

Thompson SC, Weldon RJ, Rubin CM et al (2002) Late Quaternary slip rates across the central Tien Shan, Kyrgyzstan, central Asia. J Geophys Res 107(B9):1–32

Xu XW, Zhang XK, Ran YK et al (2006) The preliminary study on seismotectonics of the 2003 AD Bachu-Jiashi earthquake (Ms 6.8), southern Tian Shan. Seismol Geol 28(2):161–178 (in Chinese with English abstract)

Yang HJ, Li YJ, Shi J et al (2010) Tectonic characteristics of the late Cenozoic south Tianshan fold-thrust belt. Quat Sci 30(5):1030–1043 (in Chinese with English abstract)

Yeats RS, Sieh K, Allen CR (1997) The geology of earthquakes. Oxford University Press, Oxford, pp 320–321